VILNIUS UNIVERSITY
CENTER FOR PHYSICAL SCIENCES AND TECHNOLOGY

ANDRIUS ARLAUSKAS

INVESTIGATION OF SEMICONDUCTOR MATERIALS AND THEIR STRUCTURES BY TERAHERTZ EXCITATION AND PICOSECOND PHOTOCONDUCTIVITY SPECTROSCOPY METHODS

Summary of doctoral dissertation
Physical sciences, Physics (02 P)

Vilnius, 2015

Doctoral dissertation was prepared in 2011 – 2015 at ultrafast Optoelectronics laboratory, Department of Optoelectronics of the Center for Physical Science and Technology.

Scientific supervisor – dr. Ramūnas Adomavičius (Center for Physical Science and Technology, Physical sciences, Physics – 02P)

Scientific consultant – prof. habil. dr. Arūnas Krotkus (Center for Physical Science and Technology, Physical sciences, Physics – 02P)

Dissertation will be defended in united Vilnius University and Center for Physical Sciences and Technology council of physical sciences:

Chairman - prof. dr. Kęstutis Arlauskas (Vilnius University, Department of Solid-state Electronics, Physics - 02P).

Members:

prof., habil. dr. Arvydas Matulionis (Center for Physical Science and Technology, Physical sciences, Physics – 02P);

Dr. Rimantas Simniškis (Center for Physical Science and Technology, Physical sciences, Physics – 02P)

Prof. dr. Valdas Pašiškevičius (Royal Institute of Technology, Sweden, Physical sciences, Physics - 02P)

Dr. Virgilijus Vaičaitis (Vilnius university, Physical sciences, Physics – 02P);

The dissertation will be defended under open consideration in the council of physics on 22th December, 2015, 3 p.m. at the Center for Physical Science and Technology, Semiconductor Physics Institute conference hall (room 206).

Address: A. Goštauto g. 11, Vilnius, Lietuva

The summary of the dissertation was distributed on November 20, 2015.

The dissertation is available in Vilnius University, Center for Physical Science and Technology libraries and in VU web site: *www.vu.lt/lt/naujienos/ivykiu-kalendorius*

VILNIAUS UNIVERSITETAS
FIZINIŲ IR TECHNOLOGIJOS MOKSLŲ CENTRAS

ANDRIUS ARLAUSKAS

PUSLAIDININKINIŲ MEDŽIAGŲ IR JŲ DARINIŲ TYRIMAS TERAHERCINĖS SPINDULIUOTĖS SUŽADINIMO IR PIKOSEKUNDINIO FOTOLAIDUMO SPEKTROSKOPIJOS METODAIS

Daktaro disertacijos santrauka
Fiziniai mokslai, fizika (02 P)

Vilnius, 2015

Disertacija rengta 2011–2015 metais Fizinių ir technologijos mokslų centre.

Mokslinis vadovas – dr. Ramūnas Adomavičius (Fizinių ir technologijos mokslų centras, fiziniai mokslai, fizika – 02P).

Mokslinis konsultantas – prof. habil. dr. Arūnas Krotkus (Fizinių ir technologijos mokslų centras, fiziniai mokslai, fizika – 02P)

Disertacija ginama Vilniaus universiteto ir Fizinių ir technologijos mokslų centro jungtinėje Fizikos mokslo krypties taryboje:

Pirmininkas – prof. dr. Kęstutis Arlauskas (Vilniaus Universitetas, Kieto kūno elektronikos katedra, Fizika - 02P).

Nariai:

prof., habil. dr. Arvydas Matulionis (Fizinių ir technologijos mokslų centras, fiziniai mokslai, fizika – 02P);

dr. Rimantas Simniškis (Fizinių ir technologijos mokslų centras, fiziniai mokslai, fiziniai mokslai, fizika – 02P)

Prof. dr. Valdas Pašiškevičius (Karališkasis technologijų institutas, Švedija, Fizika – 02P)

Dr. Virgilijus Vaičaitis (Vilniaus universitetas, fiziniai mokslai, Fizika – 02P);

Disertacija bus ginama viešame Fizikos mokslo krypties tarybos posėdyje 2015 gruodžio 22 d. 15 val. Fizinių ir technologijos mokslų centro, Puslaidininkių fizikos instituto konferencijų salėje (206 kab.)

Adresas: A. Goštauto 11, Vilnius, Lietuva.

Disertacijos santrauka išsiuntinėta 2015 m. lapkričio mėn. 20 d.

Su disertacija galima susipažinti Vilniaus universiteto, Fizinių ir technologijos mokslų centro bibliotekose *ir* VU interneto svetainėje adresu: *www.vu.lt/lt/naujienos/ivykiu-kalendorius*

Contents

Introduction

Duration of many processes occurring in semiconductors is the same as terahertz (THz) pulse – single cycle, with several picoseconds period electromagnetic oscillation. Therefore it is not surprising that these processes influence interaction between material and THz radiation. Since both THz generation and detection takes place in semiconductors, these pulses provide information about various processes in these materials.

When semiconductor surface is illuminated by femtosecond laser pulses, electromagnetic oscillation of one cycle and several picoseconds duration is generated at reflection angle, whose spectrum covers the range from a few hundred gigahertzes (GHz) to several terahertzes. The nature of this radiation depends on both: semiconductor material and parameters of femtosecond pulse. When semiconductor is transparent to the excitation wavelength, THz pulses are usually generated due to nonlinear optical effects. On resonant excitation case other mechanisms, such as plasmon oscillations coherent phonons and others, sets on. However, in most cases THz pulses are generated by free charge carriers (mostly electrons) which after photo-excitation, due to some reasons, move at different velocities and therefore current starts to flow at semiconductor surface. During the charge separation short electromagnetic pulse is generated. This charge separation mechanism is an essential process which many tries to understand and learn how to control it. There are several reasons of this separation, and sometimes it is even more than one, but the most important thing is that THz pulse has information about generation mechanism. Therefore, investigation of THz pulses not only allows analyzing various processes, occurring in the semiconductor after photo-excitation and identify number of important material parameters, but also to determine THz generation mechanism in these materials.

On the other hand, THz pulses have to be detected. Photoconductive antennas, which are made from semiconductor materials, are the most popular detectors in THz time domain spectroscopy systems (THz-TDS). Since duration of THz pulse is in order of few picoseconds, interaction between photo-excited electrons and THz pulse lasts very short period of time. This allows investigating such processes as carrier scattering to subsidiary valleys, determine their lifetime, mobility dependence on excess energy, position of defect states in the band gap. All these factors determine detected signal size and shape.

All above-mentioned processes, in THz generation and detection cases, depends on carrier excess energy. Two methods are presented in this thesis: THz excitation spectroscopy, which investigates THz pulse generation efficiency depending on the excitation wavelength, and picosecond photoconductivity spectroscopy, which alows to determine recorded THz pulse amplitude dependence on laser wavelength, which excites the detector. In order to demonstrate possibilities of these techniques, such well-known materials as GaAs, LT-GaAs, InAs and other III-V group semiconductors were analyzed. Other materials like tellurium and InAs nanowires, where mechanisms of THz generation are not well understood, were analyzed in more detail.

Main goal

The main goal of this dissertation was to develop THz excitation and picosecond photoconductivity spectroscopy methods and adapt them to semiconductors and its structures characterization.

Objectives of the study

- Measure THz excitation spectrum of III-V type semiconductors and determine subsidiary valley position of conduction band from them. Compare these values with already known ones.
- Investigate THz generation from InAs nanowires and crystalline tellurium by THz excitation spectroscopy and propose theoretical models explaining this generation.
- Measure picosecond photoconductivity spectra of low temperature grown semiconductors. Create theoretical model to explain these spectra and extract information about deep defective level states from these spectra.

Novelty

- Continuous THz excitation spectra of III-V semiconductors were measured and analyzed. Measurements were performed in a wide excitation wavelength range (640 - 2600 nm).
- THz pulses from catalyst free grown InAs nanowires were generated for the first time. Theoretical model explaining this generation was proposed.
- THz pulse generation mechanisms in tellurium crystals were examined in detail. Azimuthal angle dependences of THz pulse amplitude at various excitation photon energies were measured for the first time.
- Picosecond photoconductivity spectroscopy methodology was presented. Applications of this method were demonstrated by analyzing low temperature grown semiconductors.

Contribution of the author

Assembly of experimental setup and most measurement were carried out by the author. Only Fig. 6 in section 3.2 and fig. 10 in section 3.3 were obtained by other scientists. Author largely contributed to the processing of experimental results and its preparation for publication. Samples, excluding InAs nanowires, were also prepared by the author of this dissertation. Simulations presented in Chapter 4 were largely carried out by J. Adamonis.

Statements to defend

- THz excitation spectroscopy is a convenient method to determine subsidiary valley positions in semiconductors.
- Photo-Dember effect is the dominant THz pulse generation mechanism in catalyst-free InAs nanowires; THz generation efficiency depends on their diameter and length.
- THz pulses from crystalline tellurium surface, when photon energy of exciting light is smaller than 0.9 eV, are generated due to second order nonlinear effect. At higher photon energies the photo-Dember effect starts to take over.
- Picosecond photoconductivity spectrum is more informative than the usual photoconductivity spectrum. It reveals energetic position and width of deep level defect band; subsidiary valley positions of the conduction band also could be determined from this spectrum.

Chapter 1

Origin of THz pulse generation

THz generation could be understood as electromagnetic radiation by accelerating charges. There are two ways of this acceleration to manifest. First one is when bound electrons oscillate around equilibrium position. Second one is when free charges move with acceleration. Therefore THz generation mechanisms are divided into two different groups:

- nonlinear optical effects,
- current effects.

First one is related with second and third order nonlinear polarizations and often is called as optical rectification (OR) and electrical field induced optical rectification (EFIOR) respectively. As the name suggests, during the THz generation process, femtosecond optical pulse is rectified thus creating one period and similar duration as exciting pulse electromagnetic oscillation. On the other hand this phenomenon could be understood as difference frequency generation of two electromagnetic waves, which frequency difference is in THz range.

Second group involves all effects which are related with free carrier charge separation after photo excitation. Several mechanisms are responsible for it. One of it is well known photo-Dember effect [1,2], when electrons and holes separate from each other due to different diffusion coefficients. If there is built-in electric field at the semiconductor surface, this field itself is the driving force for carrier separation and therefore THz pulse generation [3]. More over carriers after photo excitation have predetermined momentum distribution, which in general case is not isotropic [4]. This initial momentum distribution and conduction band nonparabolicity leads to the formation of short current pulse, which is the source of THz radiation [5].

Chapter 2

Experimental details and methods

Most of the experiments are based on an amplified ytterbium-doped potassium gadolinium tungstate (Yb:KGW) laser system (PHAROS, Light Conversion Ltd) operating at 1030 nm with the pulse duration of 160 fs and the pulse repetition rate of 200 kHz. The average power of 6,5 W from this laser is directed into a cavity-tuned optical parametric oscillator (OPA ORPHEUS, Light Conversion Ltd) that generated 140–160 fs duration pulses with a central wavelength tunable from 640 to 2600 nm.

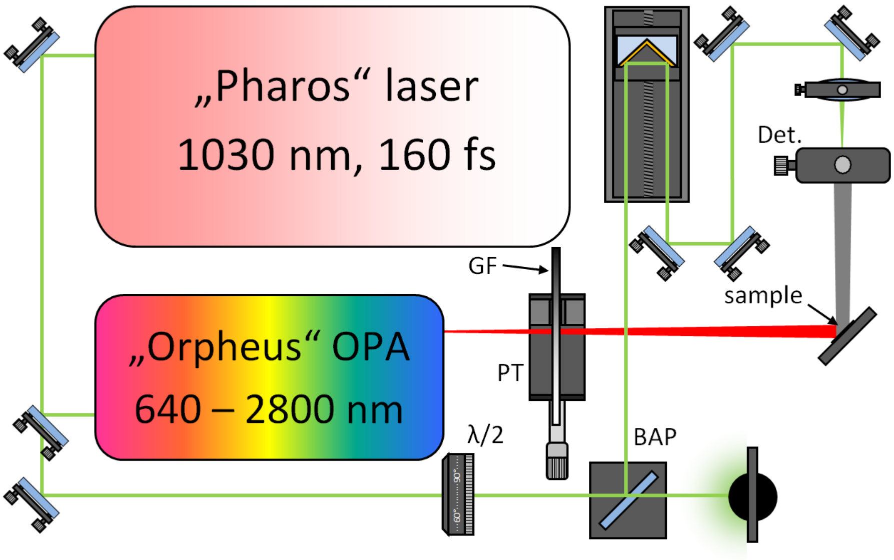

Fig. 1 Experimental set-up of THz excitation spectroscopy. Det. – GaAsBi photoconductive detector, GF – neutral density gradient filter, PT – positioning table, λ/2 – half-wavelength plate, BAP – Brewster's angle polarizer

2.1 THz excitation spectroscopy

Figure 1 demonstrates THz excitation spectroscopy set-up. It is regular THz-TDS arrangement activated by above described laser system. Investigated surface emitters were excited with the output beam from OPA. Radiated THz signals were detected in a photoconductive antenna manufactured from the GaAsBi epitaxial layer. It was illuminated by a small part of the Yb:KGW laser beam, whose power was reduced to ∼1 mW by two beam splitters. Detector beam was delayed by different time with respect to the optical beam activating THz emitter. Radiated THz pulse shapes were determined by measuring the photocurrent induced in the detector with a lock-in amplifier at different delays. THz excitation spectrum was obtained by measuring THz pulse waveform at different laser excitation wavelengths and plotting THz amplitude dependence on it.

2.2 Picosecond photoconductivity spectroscopy

This set-up is very similar to that, which is demonstrated in figure 1. The only difference is that surface emitter – p-InAs – was photoexcited with a part of the Yb:KGW laser beam with an average power of 380mW. On the other hand, photoconductive detectors, which were made from investigated materials, were activated with variable wavelength femtosecond pulses from the OPA. As the electrical bias of the photoconductor was the same in all cases – the THz pulse emitted by the InAs crystal – the lock-in amplifier signal was proportional to the detector photoconductivity integrated over the bias pulse duration.

Though dipole antenna is distorting THz pulses incoming to the photoconductor, but their duration remains quite short, of the order of 0.5 ps. As this time is shorter than the electron energy relaxation time [6], the bias pulse will sample photoconductivity of the sample at the initial stages of electron dynamics after their excitation with femtosecond laser pulses. Thus photoconductivity several picoseconds after photoexcitation is measured.

2.3 Optical pump and generation probe

The last set-up is similar to that demonstrated in figure 1 and was used to determine electrical field dynamics in semiconductor surface after photoexcitation. In this experiment, the samples are excited by two femtosecond optical beams of different wavelength coming from the OPA system: a part of 1030 nm wavelength beam generated by the laser (probe beam) and variable wavelength beam from the OPA (pump beam). The probe beam is mechanically chopped, and the THz pulse amplitude dependence on delay between pump and probe pulses is measured.

Chapter 3

THz excitation spectroscopy

3.1 III-V group semiconductors

THz excitation spectra of four different semiconductors – InAs, InSb, InN, GaAs – will be presented in this section. The main purpose of this section is to demonstrate that this method is a great tool for analysis of semiconductors band structure: mainly for determination of subsidiary valley position of conduction or valence bands.

InAs

Czochralski grown p-type and n-type InAs (hole and electron concentrations of 1.3×10^{17} cm^{-3} and 8×10^{17} cm^{-3}, respectively) crystals with (111) crystallographic orientation were analyzed in this experiments.

Origin of THz generation from bulk p-InAs surface probably is related to optical orientation of photo-excited carriers [7]. According to this mechanism, carriers after excitation have predetermined momentum and moves ballisticaly for few hundred femtoseconds. Higher electron velocity results in charge separation and thus rapid current pulse at semiconductor surface appears, therefore electromagnetic oscillation in THz range is radiated. Moreover nonparabolicity of conduction band results in creation of current parallel to the surface, which has larger escape factor of THz radiation.

Fig. 2 presents the dependence of the THz pulse amplitude generated by p-type InAs on the laser quantum energy. Clear maximum at $h\nu \approx 1.64$ eV is present in this dependence. Its origin is related to the onset of electron scattering to the subsidiary conduction band valleys at L points of the Brillouin zone, which substantially impairs the quasi-ballistic electron propagation and charge separation at the surface. Intervalley energy separation can be determined from aforesaid spectral maximum position. Taking into account intervalley phonon energy in InAs ($\hbar\omega$ = 0.027 eV), momentum conservation law and non-parabolicity of the conduction band, this separation is equal to

$$\varepsilon_{\Gamma L} = 1.11 \pm 0.04 \text{ eV}$$

and is similar to the value obtained before in [8].

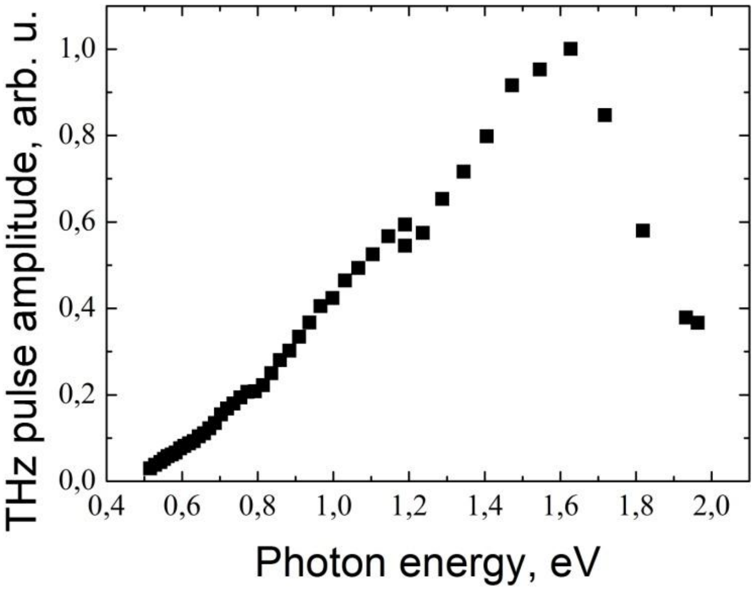

Fig. 2 THz excitation spectrum of p-InAs. Discontinuity near 1.2 eV could appear due to small experimental set-up rearrangement when changing from the signal to the idler wave

These results cannot be explained in terms of physical mechanisms solely related to the photo-Dember effect. The current surge in the surface field of p-type InAs should result in the THz pulse with a polarity opposite to that of the pulse generated due to photo-Dember effect. No such change in the radiated THz pulse polarity was observed in this experiment. The same is observed in n-InAs (not shown here). This allows us to conclude that anisotropic photoconductivity (optical orientation) is the main mechanism responsible for the THz pulse emission from InAs surfaces.

InSb

Energy bandgap of InSb is about two times narrower than that of InAs; therefore, laser quanta excite electrons with a larger excess energy, which could facilitate carrier separation and more intense THz pulse generation from that material. However, a narrow ε_g also results in a higher level of the conduction band non-parabolicity, so the electron group velocity in InSb starts to saturate earlier than in semiconductors with wider bandgaps. Moreover, intervalley energy separation in the conduction band of InSb is two times smaller than that of InAs leading to the disturbance of photoexcited electron quasi-ballistic propagation at smaller excess energies. Both these factors significantly limit the efficiency of the THz pulse generation at the InSb surface. Nevertheless, InSb is still a rather efficient THz emitter when excited with femtosecond laser pulses at wavelengths from the technologically important 1.5 μm range [9].

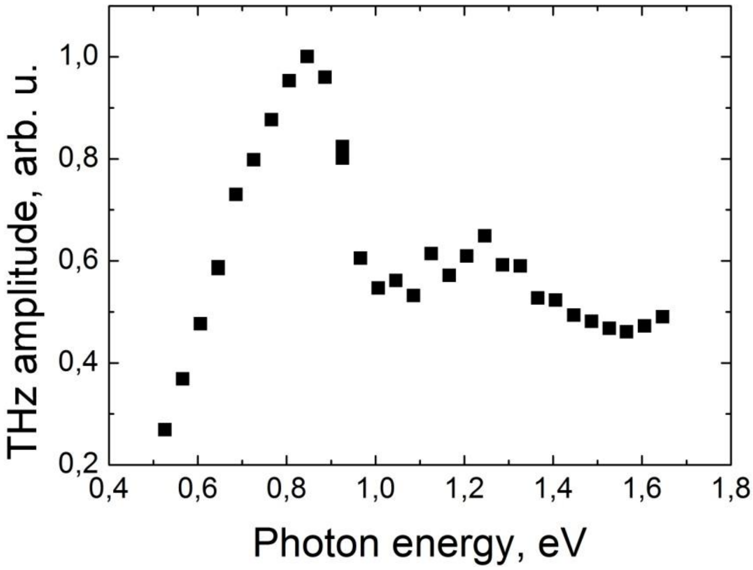

Fig. 3 THz excitation spectrum of InSb

The dependence of the radiated THz pulse amplitude on the photon energy measured at room temperature on the (111) surface of intrinsic InSb is presented in figure 3. The shape of the THz excitation spectrum of InSb is more complicated than that in the case of InAs. First maximum at $h\nu$=0.88 eV corresponds to the case when the excess energy of electrons excited from the heavy-hole band is sufficient for electron transfer into subsidiary L valleys. Taking into account conduction band non-parabolicity, separation between Γ and L valleys is:

$$\varepsilon_{\Gamma\mathrm{L}} = 0{,}55 \pm 0{,}03 \text{ eV}.$$

Second maximum, at photon energies of ~1.3 eV, possible is related with the inter-valley scattering of electrons excited from the light-hole valence band. Indeed, if one assumes that the dispersion laws of the conduction and the light-hole bands have symmetric shapes, both the electron and the light-hole will have excess energies equal to

$$\varepsilon_{\mathrm{ex}} = \frac{h\nu - \varepsilon_{\mathrm{g}}}{2}.$$

After inserting the value of InSb bandgap ε_g =0.18 eV into this equation we obtain the excess energy of electrons excited from the light-hole band equal to 0.54 ± 0,03 eV which gives the energy separation between Γ and L valleys coinciding with this value evaluated from the position of the first maximum of the THz excitation spectrum in InSb.

InN

InN has an energy band gap of less than 0.7 eV; this material was, for the first time, investigated as a surface emitter excited with Ti:sapphire laser pulses in [10]. Two physical mechanisms of THz pulse emission in InN are identified: photocurrent surge and optical rectification, and their contributions to the generated signal can interfere destructively [11].

Here InN sample grown by MOCVD technique on the sapphire substrate was investigated. Its thickness was 200 nm and electron concentration — 2.9×10^{19} cm^{-3}.

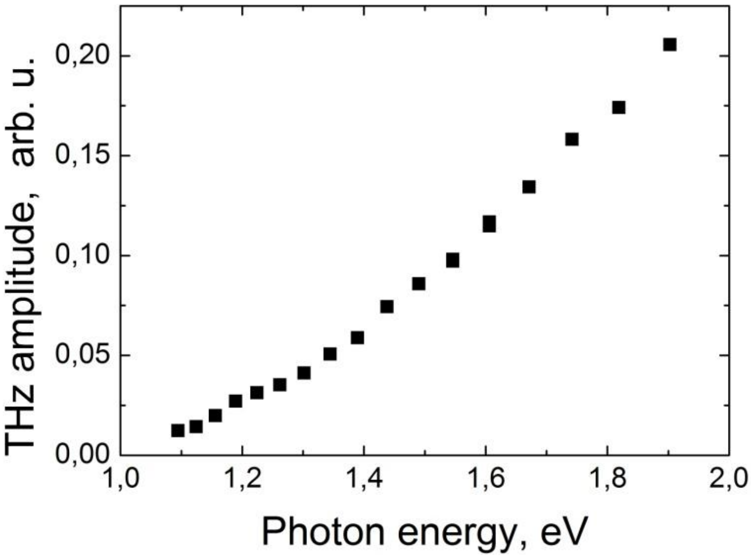

Fig. 4 THz excitation spectrum of InN

Figure 4 shows spectral dependence of THz emission generated from the InN surface. Though band gap of this material is 0.7 eV, THz pulse appears for photon energies $h\nu \geq 1$ eV. This could be explained by Moss-Burstein shift (electron fills up lower energy states in conduction band and therefore band gap for optical radiation appears to be higher). Optical band gap of InN for $n = 2.9\times10^{19}$ cm^{-3} approximately is 1.1 eV [12]. This value coincides very well with onset of THz excitation spectrum.

The absence of a maximum in the THz amplitude dependence on the laser photon energy evidences that intervalley separation in the conduction band of InN is larger than that in other investigated semiconductors. The lower limit for this separation can be estimated to be 1.1 eV; thus InN could be a promising material for surface THz emitters activated with short wavelength femtosecond lasers.

GaAs

GaAs is wide band gap semiconductor which ε_g is 1.42 eV. Most authors agree that when the surface of this semiconductor is excited with Ti:sapphire laser pulses (800 nm), the main mechanism responsible of THz pulse generation is the current transient induced by surface electric field [13]. Larger photon energy increases carrier excess energy. Due to this diffusion [14] and optical orientation currents becomes more rapid, this results in larger terahertz pulse amplitude.

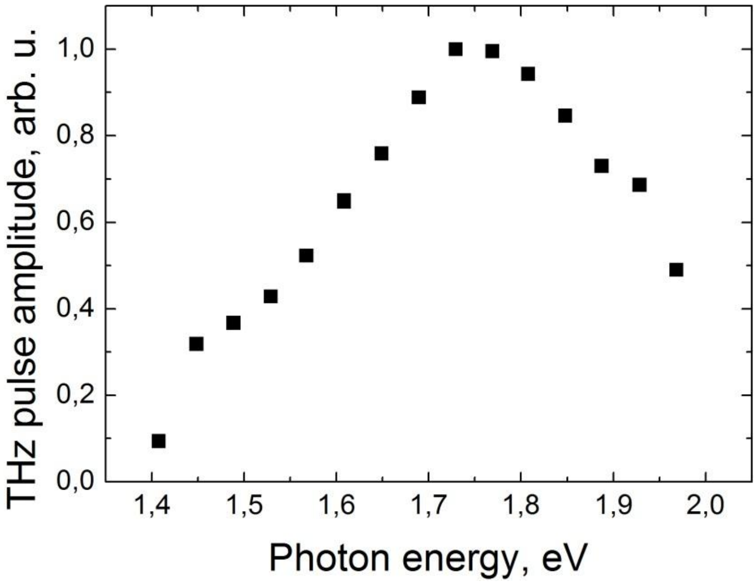

Fig. 5 THz excitation spectrum of GaAs

THz excitation spectrum of GaAs is shown in Figure 5. It can be seen that THz generation begins almost instantly when the photon energy is equal to the semiconductor ε_g. In this part of the spectrum, THz pulses are generated due to surface electric field, which accelerates the carrier even when electron excess energy is low. Further increase of kinetic energy leads to larger THz amplitude due to optical orientation and/or photo-Dember effect. This shows that the latter mechanism and surface electric field creates THz pulses of the same polarity. In other words, the conduction band is bent upwards.

When photon energy reaches 1.75 eV electron scattering to subsidiary L valleys takes place. Since GaAs conduction band is parabolic, energy distance between Γ and L valley is

$$\varepsilon_{\Gamma L} = 0.32 \pm 0.04 \text{ eV}.$$

Scattering to X valley, which is 0.48 eV above the bottom of conduction band [15], should begin at 1.95 eV. Larger inclination at the end of the spectrum probably attests that. In order confirm that, measurement at larger photon energies must performed.

3.2 THz pulse generation from InAs nanowires

Simple excitation geometry, wide range of excitation wavelengths and high signal-to-noise ratio are very attractive features of the surface THz emitters in TDS systems. Nevertheless, its radiation intensity is too small. Even the best surface emitter – bulk p-InAs [16] – emits one order (or even more) smaller amplitude signal than the photoconductive antennas. Therefore, new materials or their derivatives which exhibit more efficient THz pulse generation are highly desirable and nanowires (NW) could be a great alternative.

Samples

The InAs NWs were grown in a completely catalyst-free, selective area epitaxial growth (SAEG) mode on SiO_2/Si templates using solid-source molecular beam epitaxy (MBE). The SiO_2/Si templates consist of commercially available 2″ p-type Si (111) wafers with a 20-nm-thick thermally grown SiO_2 dielectric mask layer prepatterned by nanoimprint lithography (NIL) [17]. The prepatterned template thus exhibits a periodic pattern of 60 nm wide holes separated by a pitch of 250 nm across an area of $\sim 8\times 8$ mm^2. This enables the growth of NWs in a site-selective, highly periodic manner with minimal size distribution and homogeneous NW densities of $\sim 2.5\times 10^9$ cm^{-2}. The as-grown InAs

NWs are intrinsically n-type with an estimated carrier concentration of ∼10^{17} cm^{-3} and electron mobilities of ∼800−2000 $cm^2/(V\ s)$ at 300 K, as derived from transconductance measurements of single back-gated NW field effect transistors [18]. In total, a series of three InAs NW samples was grown with significantly different NW lengths (i.e., aspect ratio) by adjusting the growth time (t) among 45, 125, and 200 min the average NW length and diameter increase from l = 0.75 μm/d=80nm(t = 45 min),l = 1.8μm/d= 136 nm (t = 125 min), to l = 3.3μm/d= 143 nm (t = 200 min), giving aspect ratios ranging from ∼ 9 to 23. Since obviously the NW length is the most distinctly varying parameter, later on only NW length will be referred when comparing different samples.

Experimental results and discussion

The emitted THz pulses and the corresponding Fourier spectra are shown in Figure 6 for the three InAs NW samples in comparison with a p-type bulk InAs reference ($p = 10^{18}$ cm^{-3}). We observe that the amplitude of the generated THz pulses is strongly related to the NW length and aspect ratio. In particular, by increasing NW length (aspect ratio) the amplitude of the THz pulses increases steadily, reaching a peak amplitude (at zero delay) in the sample with ∼3.3μm long NWs that is equal to ∼60% of the amplitude emitted from the p-type bulk InAs reference. The Fourier spectra of the NW-related THz pulses are presented in Figure 6b further show some interesting features with respect to bulk p-type InAs. Spectra corresponding to longer NWs (samples with l^{NW}= 1.8μm and l^{NW} = 3.3μm) are essentially equivalent to the spectrum obtained for the p-type bulk InAs reference, although their width is, most probably, limited by the temporal response of the detector used. In contrast, the Fourier spectrum of the THz pulse radiated from the other sample (l^{NW} = 0.75 μm) is distinctly narrower. This difference will be elucidated in more detail further below.

To further identify characteristic differences in THz emission from NWs and bulk excitation, wavelength-dependent TDS measurements are performed using set-up described at section 2.1. The corresponding THz excitation spectra of the three InAs NW samples together with the spectrum measured on p-type bulk InAs using an excitation fluence of ∼50 nJ/cm^2 are presented in Figure 7. First of all, the THz pulse amplitude measured on the NW samples is monotonously increasing with increasing the laser photon energy, and no spectral maximum typical for the majority of bulk III−V semiconductor crystals is observed in the range of investigated photon energies. Second, the emitted THz transient becomes stronger with increasing length of the NWs, in accordance with the observations in Figure 6.

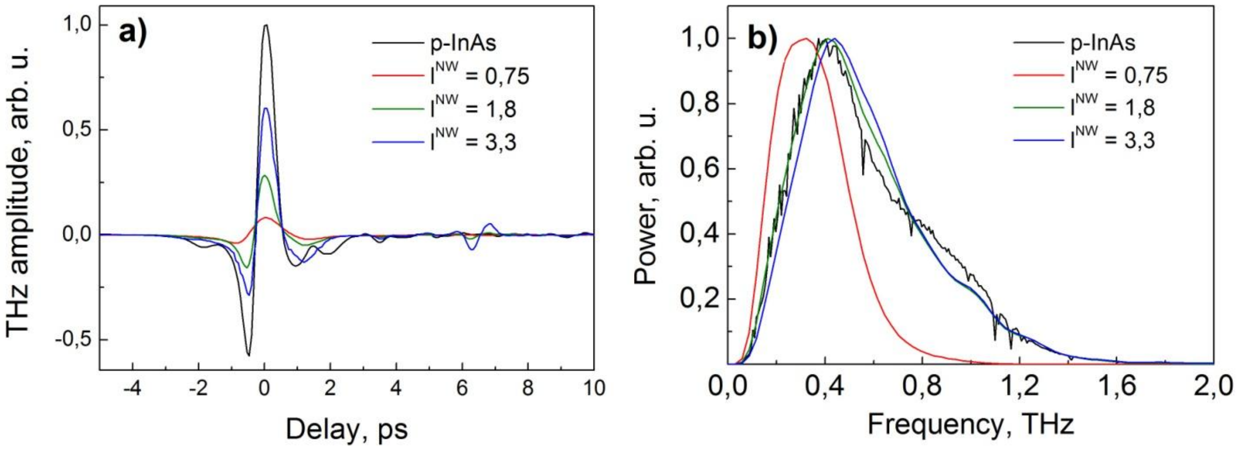

Fig. 6 THz pulses (a) and their Fourier spectra (b) radiated from the surfaces of p-type bulk InAs and three n-type InAs NW samples excited by femtosecond Ti:sapphire laser pulses and detected by LT-GaAs photoconductive antenna.

The origin of this differences most likely stems from the impaired electron mobility in intrinsic InAs NWs due to surface effects that dominate the charge carrier transport properties. Generally, electron mobility in InAs NWs with diameters from 70 to 150 nm are in the range of~800−2000 cm2/(V s) [19,20], values which are much smaller than the bulk electron mobility of InAs at room temperature (i.e., >20 000 cm2/(Vs) [21]). This means that the momentum relaxation time of electrons in NWs, $\tau_m = \mu m^*/e$, will be very short, on the order of several tens of femtoseconds. In bulk InAs, a maximum in the THz excitation spectrum appears when the excess energy of photoexcited electrons becomes comparable to the energy separation between the main Γ valley and subsidiary L and X valleys with large effective electron masses and low mobilities. Because values of τ_m in InAs NWs are comparable or even shorter than intervalley scattering times, which are on the order of ~50 fs for Γ−X scattering and ~300 fs for Γ−L scattering, the intervalley transitions will have only a minor effect on the photoexcited electron movement and on the characteristics of surface THz emission that is caused by this movement.

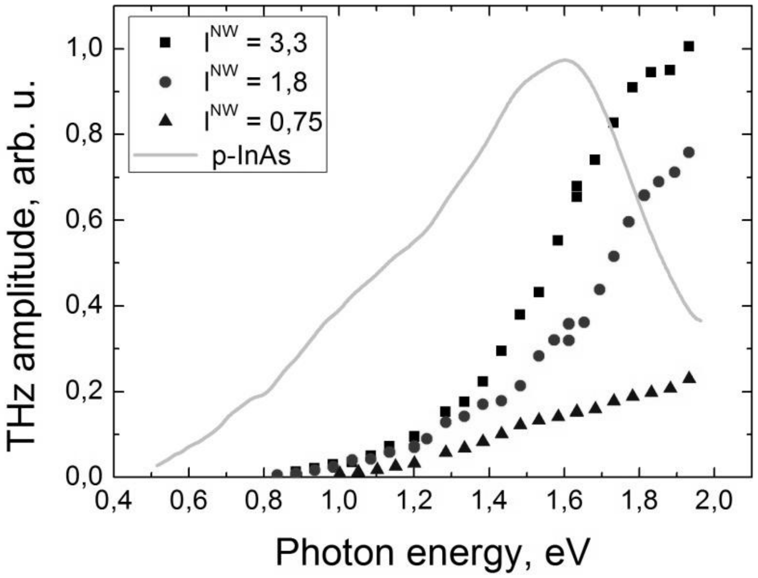

Fig. 7 THz excitation spectra of all three InAs NW samples and bulk p-type InAs reference measured under different laser photon energies with a pump fluence of ∼50 nJ/cm^2. The spectra are normalized to the same number of incident photons.

In the following, we provide a discussion and further use additional experiments to verify the underlying mechanism for THz emission in the InAs NW arrays with respect to bulk InAs. THz pulse from p-InAs surface most probably is generated due to anisotropic photo-conductivity caused by optical alignment of photoexcited electrons in a nonparabolic conduction band [5,22].

The characteristic THz radiation caused by anisotropic photoconductivity effect has a strong dependence of radiated THz field amplitude on the azimuthal angle ϕ between the crystal axes and the optical field direction. Figure 8 shows the azimuthal angle dependences measured for a p-type bulk InAs crystal cut parallel to (111) plane and for two InAs NW samples (for NWs with l^{NW} = 0.75μm and l^{NW} = 3.3μm). The recorded azimuthal angle dependences of bulk and NW samples are strikingly different. In the case of bulk InAs, the azimuthal dependence is modulated by a clear cos 3ϕ function as expected [23], whereas for the NW arrays these dependences are fully isotropic. This means that the physical mechanisms responsible for THz emission are completely different for these two cases. In particular, the anisotropic photoconductivity loses its importance in NW arrays, where the lateral movement of photoexcited electrons is restricted by the NW size (diameter) and by a much smaller momentum relaxation time than in the bulk material. Such independence of the azimuthal angle in the THz emission from semiconductor surfaces is usually attributed to one of two effects related to the origin of ultrafast photocurrent transients: A photocurrent surge due to photo-excited electron and hole separation by (i) a built-in surface field or (ii) by their different diffusion rates (i.e., so-called photo-Dember effect). Therefore in order to distinguish which one is responsible for THz generation optical pump generation probe experiment (described at section 2.3) has been performed.

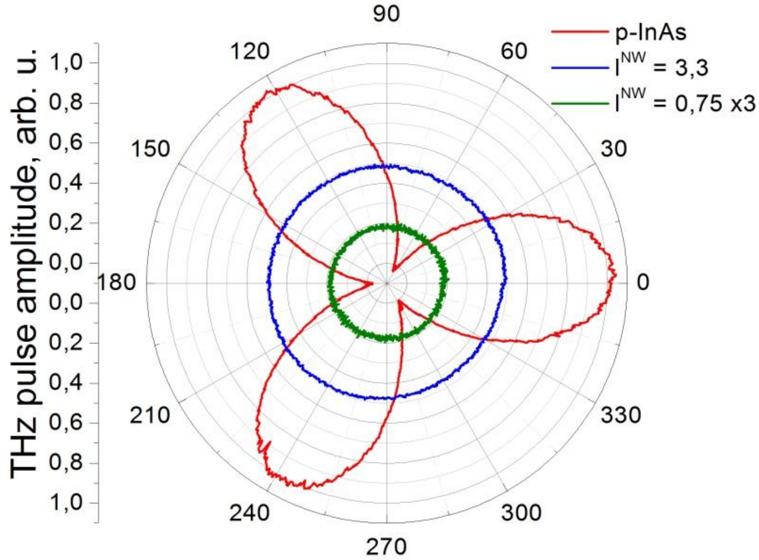

Fig. 8 THz amplitude dependence on azimuthal angle for different samples. Measurements were performed at 760 nm wavelength and 50 mW average power. The data for the sample with shortest NWs (l^{NW}=0.75μm) are multiplied by a factor of 3 to increase resolution.

The results of these measurements obtained for the p-type bulk InAs reference and an InAs NW array (sample with l^{NW} = 3.3μm) are highlighted in Figure 9 for several pump-beam wavelengths. The shape of the two-color pump-and-probe curves measured on bulk and NW samples is different at the first few picoseconds after their simultaneous excitation by two optical beams. For the bulk sample one can observe an increase of the THz pulse amplitude, whereas in contrast the NW array exhibits a reduction right at the temporal overlap of both laser pump and probe pulses (first ~5 ps). At longer delays, however, the THz signal is reduced since an electron – hole plasma created by the pump-beam causes screening effects.

Bulk p-InAs curve can be interpreted as follows: due to optical orientation charge carriers created by pump pulse moves against surface electric field thus making it stronger. Amplitude of THz radiation created by probe pulse in this amplified electric field becomes larger and therefore in Figure 9a one can notice increase of THz amplitude. Finally these charge carriers screens built-in electric field and the amplitude of THz pulse and strongly reduced.

This situation is a completely different in NW. Charge carriers created by pump pulse induces electric field in nanowires due to photo-Dember effect. Because this electric field probe pulse charge carriers separates slower. Therefore THz amplitude decreases and even changes its sign when pump pulse central wavelength becomes equal to 700 nm (Fig. 9b). Finally, electric field starts to decrease, because charge carriers acted by their own generated field returns back, therefore after a sharp decline THz amplitude starts to growth until settles at fixed value. Moreover charge carrier separation is more effective when excitation wavelength is smaller, i. e. electron excess energy is higher. That is the reason why THz amplitude grows together with photon energy in figure 7. If surface electric field would be the cause of THz generation, separation of charge carriers would result in reduced electric field and therefore only decrease of THz amplitude to a fixed value would be visible in optical pump generation probe dynamics.

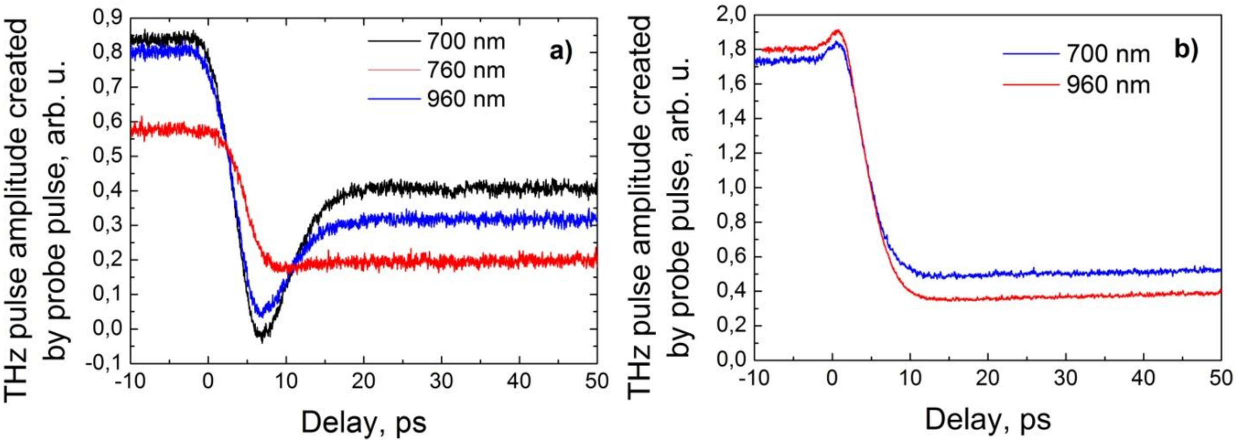

Fig. 9 THz pulse amplitude dependence on the delay between pump and probe pulses for different pump wavelengths: (a) bulk p-type InAs and (b) InAs NW array (sample with lNW = 3.3µm). Average pump and probe beam powers are 75 mW and 18 mW, respectively. The probe wavelength was 1030 nm for all measurements.

3.3 THz pulse generation from tellurium crystal

Tellurium – Group VI element that crystallizes into hexagonal lattice, where atoms are arranged helically around the so called c axis. It is one element semiconductor crystal with the greatest atomic number; therefore its phonon frequency (2.78 THz) is easily accessible by standard TDS system.

Though origin of THz generation from this material was thoroughly investigated earlier [24], several questions regarding the origin of the physical mechanism of THz emission from photoexcited Te surface is still unanswered. First of all, Te is a highly anisotropic crystal; therefore, studies of THz emission from the surfaces with different symmetry and measurements of its dependences on the angle between the optical field direction and the crystalline axes would be highly desirable. Second, the electron energy band structure of this material is very complicated and has subsidiary valleys both in the conduction [25] and in the valence band. [26] Moreover, the very presence of the photo-Dember effect in tellurium is questionable even when photocarriers are excited at the vicinity of the fundamental band gap, because the equilibrium electrons are only about 2 times more mobile than the holes [26].

Samples

Several Czochralski grown crystals of Te having the hole densities at liquid nitrogen temperature of (0.5 - 1) 10^{15} cm^{3} and their mobilities in the range from 4000 cm^{2}/Vs to 5000 cm^{2}/Vs were investigated. THz emission from the surfaces perpendicular and parallel to the c axis (hexagonal indexes (0001) and (1010), simplified indexes (001) and (100), respectively) as well as from a cleaved (102) (hexagonal index—(1012)) crystalline plane was measured.

Experimental results and discussion

Figure 10 presents THz radiation pulses and their Fourier spectra emitted from two Te samples excited by 70 fs duration Yb:KGW laser pulses (excitation power was equal to 800 mW). Distinctive characteristics of THz signals emitted by (102) orientation Te samples are the oscillations observed after the main pulse and spectral peak in the vicinity of 2.8 THz frequency, which were explained previously by the coherent phonon contribution [24]. On the other hand Fourier spectra of (001) orientation sample is different. Dipole, which oscillates in parallel to c axis, does not radiate perpendicular to its dipole moment; moreover refraction index (and reflection coefficient) varies greatly at the phonon frequency, therefore instead of peak clear pit is visible.

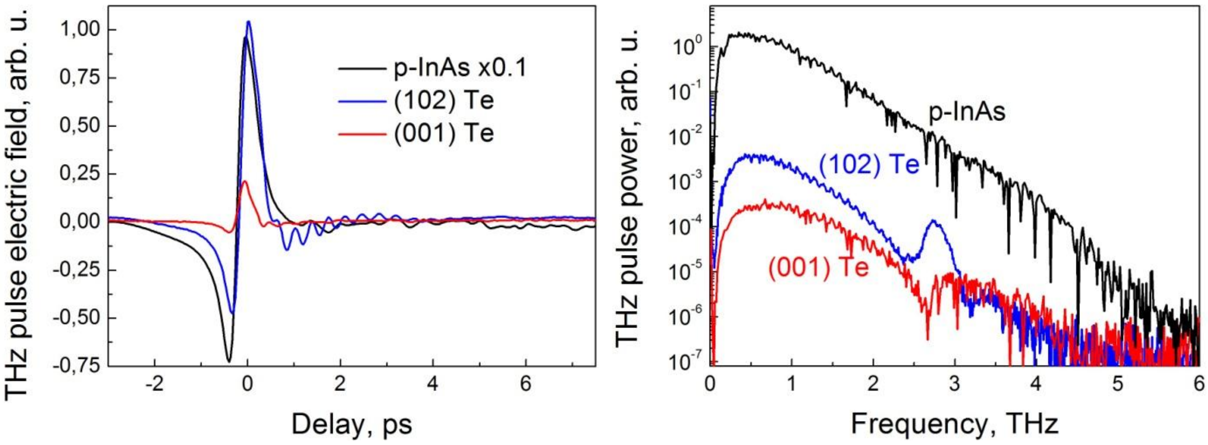

Fig. 10 THz pulses (a) and their Fourier transform spectra (b) for p-type InAs crystal and two differently cut tellurium samples.

Surface THz emission is stronger when the symmetry of the photoexcited crystal plane is lower. Figure 11 shows the dependencies of radiated THz pulse amplitude as a function of femtosecond OPA photon quantum energy for three different symmetry surfaces of Te crystal. For all three crystal orientations, THz pulses generated at the low photon energy side of the spectra are weak; their fast increase starts when the photon energy becomes larger than 0.9 eV.

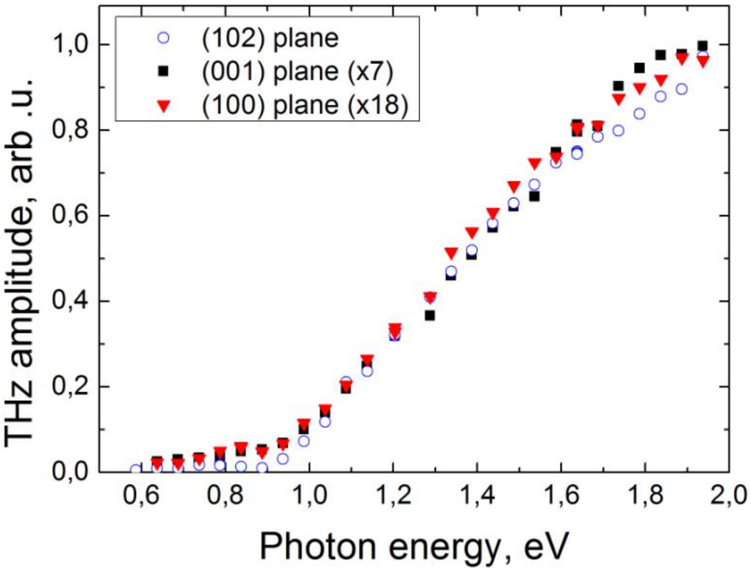

Fig. 11 THz excitation spectra measured on three Te crystal planes.

The latter value is meaningful when we consider the energy band structure details of tellurium. Direct energy band gap of Te at points H of the Brillouin zone is equal to 0.34 eV [26]. At 0.11 eV below the valence maximum there is so called P-band [26] with effective hole mass and mobility of a similar order of magnitude as in the main valence band maxima. Additional energy valleys are present in the conduction band of Te, too [27,28]; however, the effective electron mass in these valleys (lying at A or M points of the Brillouin zone) is much larger than in the lowest H minima [23]. Intervalley separation in the conduction band of Te is estimated in that work as 0.35 eV. The sum of these three characteristic energies is equal to 0.8 eV. Photon energy necessary for initiation of electron and hole transfer to secondary conduction and valence band valleys will be slightly higher both due to the electron momentum conservation and intervalley phonon emission. It is realistic to assume, that experimentally observed characteristic energy of 0.9 eV is an indication of the onset of such transfer processes.

One could also expect that the prevailing physical mechanisms of the surface THz emission in these two spectral ranges: at longer and shorter than 1.4 μm (0.9 eV) wavelengths, are different. Measurements of azimuthal angle dependences of surface THz emission from tellurium crystals were performed for the identification of these mechanisms. Figures 12 and 13 show azimuthal angle dependences measured on all three differently oriented Te samples at photoexcitation wavelengths corresponding to both these spectral ranges. Experiments were performed by using s-polarized OPO beams at 45° incidence angle; p-polarized THz signals were recorded by rotating the samples around their surface normal.

Azimuthal angle dependences for these two spectral ranges are very different. At longer than 1.4 μm wavelengths, these dependences are dominated by cos 3ϕ (or cos 2ϕ for (100) cut sample) type periodic components, which gradually evolves into cos ϕ type dependence as the laser wavelength becomes shorter. Different periodicity reflects distinct generation mechanisms. There are three of them: third order optical nonlinearity which has cos 3ϕ dependence, lateral photo-Dember effect with cos ϕ periodicity and ordinary angle independent photo- Dember effect.

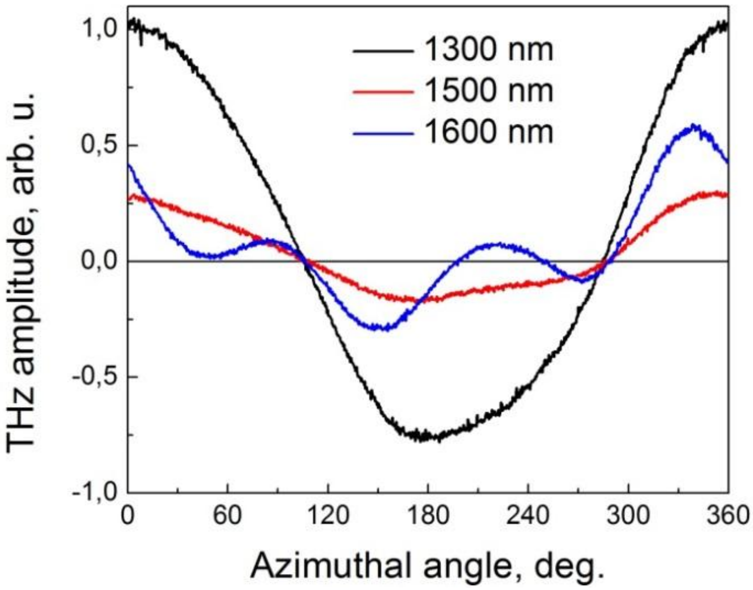

Fig. 12 Azimuthal angle dependences of THz pulse amplitude measured on (102) orientation Te on three different excitation wavelength.

Azimuthal angle independent component is, most probably, originating from dynamic polarization caused by different diffusion of electrons and holes away from the photoexcited surface – the photo-Dember effect. However, as it has been pointed above, its onset at larger than 0.9 eV photon energies, at which the electrons are scattered to the subsidiary large effective mass valleys and therefore should have lower diffusion coefficient than the holes. The measurement reveals (not shown here) that polarity of THz pulses radiated from Te surfaces is the same as from p-GaAs. This indicates that the same type carriers move towards the bulk in both cases – for tellurium crystal, it means that more mobile carriers are holes.

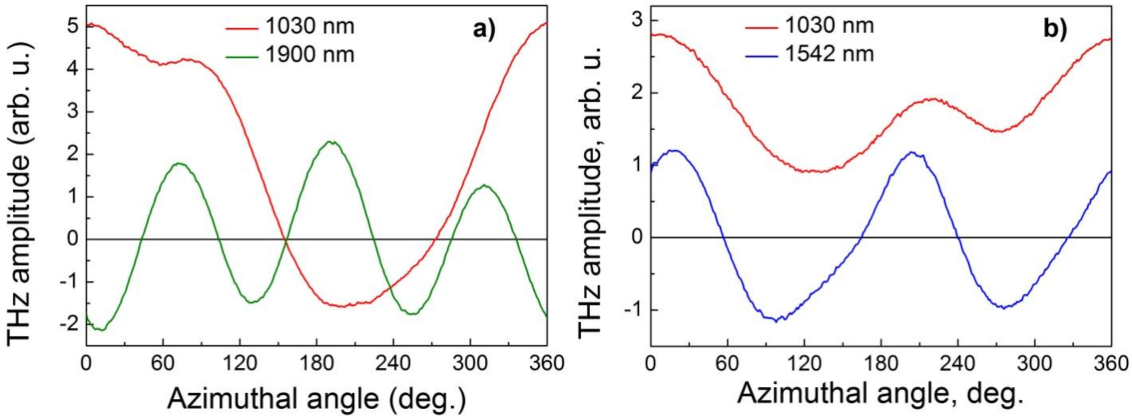

Fig. 13 Azimuthal angle dependences of THz pulse amplitude measured on Te samples with c-axis perpendicular (a) and parallel (b) to the photoexcited surface. Measurements were performed with femtosecond optical pulses with wavelengths shorter and longer than 1.4 µm.

Azimuthal angle dependence proportional to cos ϕ can be observed in the case when the radiating dipole has a built-in direction in the sample and is rotating with it. Such situation can arise for the case of so-called transverse Dember effect that was discovered in tellurium and other anisotropic crystals long time ago [28]. When the surface of an anisotropic semiconductor is exposed to light that is strongly absorbed, a carrier-concentration gradient normal to the sample surface is formed and this is accompanied by the diffusion of excess carriers into the bulk. As a consequence of electron effective mass anisotropy, however, the diffusion of electrons generally proceeds in a direction different from that of holes. Because of this, an electric current flows and a dynamic polarization can develop along the specimen surface. Transverse Dember effect is strongest for (102) tellurium sample because the carrier density gradient does not coincide with the main axes of isoenergetic surfaces of the rotation ellipsoids of Te energy dispersion law. It should also be present, although on a weaker scale, for two other crystallographic planes.

The third THz field component evident from its azimuthal angle dependences probably has a similar origin as in other semiconductors, which THz pulse amplitude depends on azimuthal angle. Phenomenologically, they are described in terms of the second or third order optical nonlinearities; their microscopical origin stems from the anisotropy of dynamic photoconductivity caused by ballistically moving optically oriented carriers [29]. Such nonlinear effects were also observed in tellurium before; they were interpreted as the optical rectification [30] or the photogalvanic effect [27]. Following the methodology presented in Ref. 31, it was calculated that for (100) cut samples azimuthal angle dependence is proportional to cos 2ϕ and for (001) – cos 3ϕ.

Chapter 4

Picosecond photoconductivity of low temperature grown semiconductors

An ordinary photoconductivity spectrum is obtained by measuring current strength flowing through the sample dependence on continuous light source wavelength. Energy band gap, impurity and defect states in the band gap and other parameters can be determined from this spectrum. However, it is difficult to measure photoconductivity of materials with short carrier lifetime, since excited charge carriers recombine very fast and therefore is not involved in current flow. Moreover, the rapid processes such as scattering to the side valleys are not visible in normal photoconductivity spectrum. Meanwhile, the methodology presented in this section does not have such drawbacks and therefore can be used for more detailed investigation of aforesaid materials.

Picosecond photoconductivity methodology will be presented in this section. In order to demonstrate its benefits three different materials with short carrier lifetime were analyzed: low-temperature grown GaAs (LTG-GaAs) and InGaAs (LT-InGaAs), GaAsBi.

4.1 LT-GaAs and LT-InGaAs

Optical properties of LTG GaAs in the spectral range below the absorption edge are critically dependent on characteristics of the As_{Ga} defect band, however, the parameters of this band, including its energy position or its width, are known rather insufficiently. For example, the activation energy for the deep As_{Ga} donor provided in the literature ranges from 0.57 [32] to 0.82 eV [33] depending on the experimental technique used to determine this parameter. We study the defect band influence on picosecond photoconductivity spectra of THz detectors made from moderately annealed LTG GaAs and $Ga_{0.7}In_{0.3}As$ (E_g = 0.97 eV) layers. These spectra were measured by using a tunable wavelength femtosecond laser system described in section 2.3.

Samples

Photoconductive THz detectors were manufactured from 1.4 μm thick LTG GaAs layers grown on a semi-insulating (SI) GaAs substrate in a solid-state molecular-beam-epitaxy reactor at a temperature of 250° C and at the beam-equivalent As/Ga pressure (BEP) ratio of 20. The layers were post-growth annealed for 30 s in a rapid-thermal-annealing oven at a temperature of 400° C. A 1.8 μm thick GaInAs layer was also grown on a SI GaAs substrate. In order to reduce lattice missmatch, InAlAs buffer was introduced during growth procedure. The growth temperature in this case was equal to 200° C and the As/Ga BEP ratio was 10. Coplanar Hertzian dipole antennas with a photoconducting gap of 10–15 μm between Ti-Au electrodes were manufactured from these layers. In order to collimate the THz radiation, all antennas were equipped with hemispherical high resistivity Si lenses.

Results

Figure 14 shows photoconductivity spectra of LTG GaAs measured by continuous light and femtosecond pulse excitation. Both spectra show the presence of a significant photoconductivity at photon energies lower than the optical absorption edge for GaAs of ~ 1.4 eV. The origin of this sub-bandgap photoconductivity is most probably electron transitions from deep donor states typical of GaAs layers grown at a low-temperature by MBE. A possible two photon absorption (TPA) contribution to the photoconductivity at these wavelengths is rather small because absorption coefficient at fluencies of $P_{opt} = 7 GW/cm^2$ is about 20 times smaller [34,35]. It has to be pointed out that the magnitude of picosecond photoconductivity in the LTG GaAs sample increases with the increment of photon energy reaching its maximum value at λ = 1 μm, which is only two times lower than at λ = 800 nm corresponding to the central wavelength of the Ti:sapphire laser spectrum. Further the decrement of picosecond photoconductivity is observed in the range between 1.2 and 1.4 eV. In this range, photons have sufficient energy for the electron excitation from the defect band to the subsidiary valleys, where electron mobility is much smaller [36] compared with value in Γ valley [37].

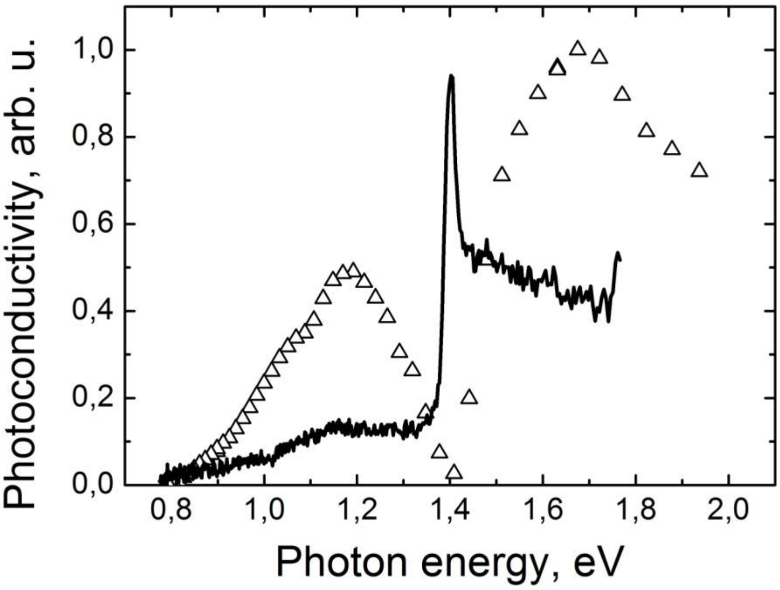

Fig. 14 Photoconductivity of the LTG GaAs sample measured under excitation with femtosecond laser pulse (triangles) and constant excitation (solid line).

At larger photon energies (>1.4 eV), the results of constant and pulsed illumination measurements are considerably different. The pulsed photoconductivity spectrum is monotonous up to the photon energy of $h\nu \approx 1.7$ eV where the onset of photoexcited electron transitions to subsidiary low-mobility conduction band valleys occurs. Whereas the photoconductivity measured by using constant excitation in that spectral range becomes very weak. Its peak observed in the vicinity of the energy bandgap is due to the photoconductance of the mobile and long living carriers excited at the thick substrate. With the increment of photon energy, the absorption coefficient of the crystal increases, at the same time reducing the absorption length of the radiation. When absorption length becomes comparable with thickness of LTG GaAs layer, the photoconductivity of short living and less mobile carrier excited at LTG GaAs layer start to dominate, leading to sufficient decrement in observed photoconductivity. The shape of the picosecond photo-conductivity dependence on the photon energy is much more complex and possibly could be used for evaluating the energy position and other parameters of the deep defect levels. Such an evaluation based on the comparison of experimental and theoretical data will be presented in the following section of this paper.

Comparison with the modeling

The terahertz pulse emitter in our experiment was a p-type InAs crystal, which radiated THz pulses of the order of 0.5 ps. As this time is shorter than the electron energy relaxation time [18], the bias pulse will sample photoconductivity of the sample at the initial stages of electron dynamics after their excitation with femtosecond laser pulses.

In this model the photoconductivity was calculated as a product of the photoexcited electron concentration and their mobility. As it was sampled in the experiments for the duration shorter than the electron energy relaxation time, a monoenergetic approximation was used in modeling [38]. The electron mobility in the conduction band was assumed to be dependent on their excess energy $\varepsilon_{\mathrm{ex}} \approx 0.9(h\nu - \varepsilon_{\mathrm{g}})$. Two main electron scattering mechanisms were taken into account: scattering by ionized ($\mu_{\mathrm{ion.}}$) and neutral ($\mu_{\mathrm{neu.}}$) impurities. The resulting electron mobility was determined by using the Mathiesen rule [39].

The energy dependence of electron mobility dominated by ionized impurity scattering was taken into account as in Ref. 34:

$$\mu_{\mathrm{ion.}} = \mu_0 \left(\frac{\varepsilon_{\mathrm{ex}}}{k_{\mathrm{B}}T}\right)^{1.5}, \tag{1}$$

with the mobility of electrons at the bottom of the conduction band μ_0 equal to 140 cm^2/Vs. $\mu_{\mathrm{neu.}}$ was calculated according to Ref. 20. Where $\varepsilon_{\mathrm{ex}}$ became larger than the energy separation between the main Γ and subsidiary L and X valleys of the conduction band, the electron redistribution between these valleys was taken into account by considering that the occupation of a particular group of valleys is inversely proportional to corresponding intervalley scattering time $\tau_{\Gamma\rightarrow\mathrm{L}}$ or $\tau_{\Gamma\rightarrow\mathrm{X}}$,

$$\frac{1}{\tau_{\Gamma\rightarrow i}} = \frac{n_{\mathrm{i}} D_{\mathrm{i}} m_{\mathrm{i}}^{3/2}}{\sqrt{2}\pi\hbar^3\omega_0\rho}\sqrt{\varepsilon_{\mathrm{ex}} - \varepsilon_{\mathrm{i}}}, \tag{2}$$

where *i* marks L or X valleys. n_{i} is the number of equivalent L or X valleys; D_{i} is the deformation potential for intervalley transitions from Γ to L or X valleys; m_{i} is the electron density of states mass; $\hbar$ is the Planck's constant; ω_0 is the phonon frequency; ρ is the mass density; and ε_{i} is the inter-valley energy separation in the conduction band.

On the other hand, the density of states distribution in the defect band was approximated by a Gaussian function

$$N_{\mathrm{def}} = N_0 \exp\left(-\frac{(\varepsilon_{\mathrm{def}}-\varepsilon)^2}{2\Delta\varepsilon_{\mathrm{def}}^2}\right), \tag{3}$$

where N_0 is the number of defect states at its maximum corresponding to the $\mathrm{As_{Ga}}$ defect energy $\varepsilon_{\mathrm{def}}$ and $\Delta\varepsilon_{\mathrm{def}}$ is the halfwidth of the defect band. The absorption coefficient for electron transitions from the defect band to the conduction band at the photon energy $h\nu$ was found by summing-up the product of Eq. (3), the optical absorption cross-section, and the density of states in the conduction band at $\varepsilon_{\mathrm{ex}} = h\nu - \varepsilon$ over all possible final electron energies $\varepsilon_{\mathrm{ex}}$. For the electron excitation above the subsidiary valleys, direct transitions from the defects to these valleys were assumed. The number of electrons excited from the defects to Γ, X, and L valleys was assumed to be proportional to the corresponding density of states in each valley group at a given energy.

In figure 15, experimental and theoretical picosecond photoconductivity spectra of LTG GaAs and LTG GaInAs in the whole investigated wavelength range are compared. In the case of LTG GaAs (Fig. 15a), the coincidence between experimental and calculated spectra is quite good, especially when one takes into account a rather rough theoretical model is used. The best match between the experimental results and the simulation was achieved for $\varepsilon_{\mathrm{def}} = 0.77\mathrm{eV}$ and $\Delta\varepsilon_{\mathrm{def}} = 78\mathrm{meV}$.

Similar experiments and modeling were also performed with LTG GaInAs samples (Fig. 15b). The coincidence between the experimental results and modeling in this case is even better than for LTG GaAs. The sub-bandgap, the defect-related photoconductivity part of the LTG GaInAs, spectrum is observable quite clearly, the only difference from LTG GaAs is that the maximum related to the onset of intervalley transfer is overlapping with the inter-band part of the spectrum. Fitting of the calculated results with the experimental data gives the defect band position in this material to be 0.4 eV with bandwidth similar to LTG-GaAs and the Γ–L inter-valley energy separation of 0.68 eV. It should be pointed out that in as-grown LTG $\mathrm{Ga_{0.7}In_{0.3}As}$, a significant photoconductivity signal was observed at even longer wavelengths than in LTG GaAs, the photosensitivity spectrum of this material was covering another technologically important spectral range of 1.5 μm.

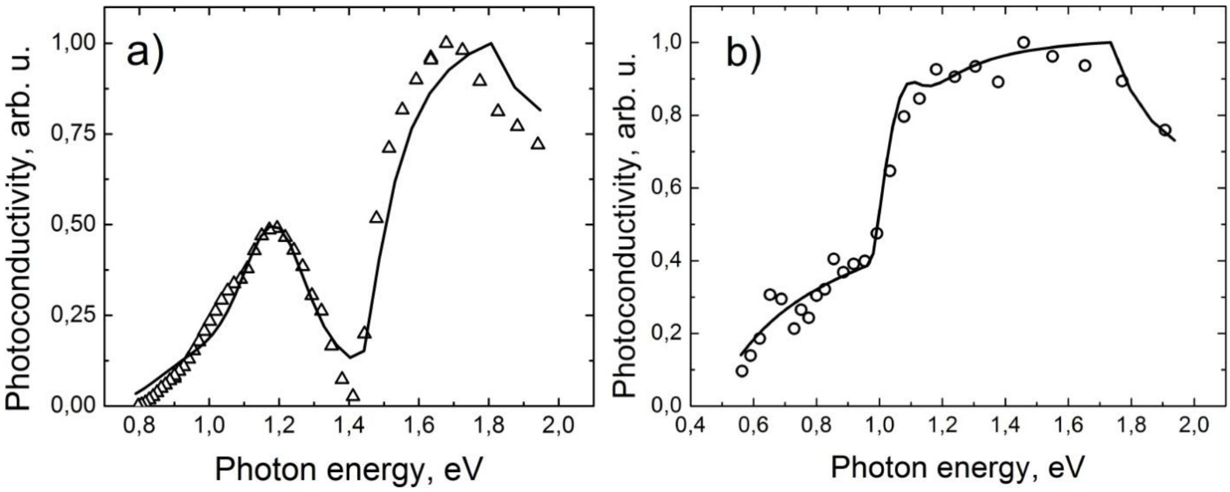

Fig. 15 Measured picosecond photoconductivity spectra (points) and their theoretical fits (lines) in: (a) LTG GaAs, (b) LTG GaInAs.

4.2 GaAsBi

GaAsBi is one of the few substances that are photosensitive at larger than 800 nm wavelength and at the same time have similar characteristics as the LTG GaAs: high dark resistivity and electron mobility and short carrier lifetime (<1 ps). It has been demonstrated previously that GaAsBi is suitable material for photoconductive antennas, which are activated by a 1 μm central wavelength femtosecond pulses [40]. In this section picosecond photoconductivity spectrum of GaAsBi will be discused. THz-TDS system activated by 1.55 μm femtosecond laser system also will be demonstrated.

Samples

Two GaAsBi layers were grown on the semi-insulating (100)-oriented GaAs substrate in a molecular beam epitaxy system with solid-state sources at 240° C at the growth rate of 2 μm/h and at different Bi/As beam ratios. The thickness of the layers was 1.5 μm. The bismuth content in both layers as determined from X-ray diffraction spectra was about ~6%; energy band gaps of the GaAsBi alloys estimated from the optical absorption edge were 0.95 eV for layer A grown at a lower Bi-beam pressure and 0.9 eV for layer B grown at a larger Bi-beam pressure. Electron lifetime was measured by optical pump–THz probe experiment and in samples A and B it was equal to 1.7 and 1.3 ps respectively. Electron mobility of about 2000 cm^2V^{-1} s^{-1} was estimated from the same experiment in both samples. GaAsBi layers were used for manufacturing a planar 70-m-wide Hertzian dipole antennas with the 10-μm-wide photoconducting gaps between Ti–Au electrodes; the antennas were equipped with the hemispherical lenses made from a high resistivity silicon crystal.

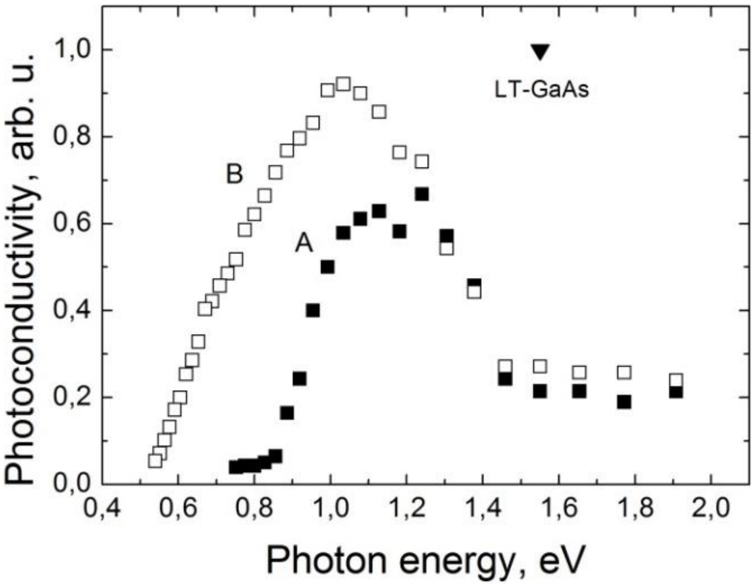

Fig. 16 Detector sensitivity dependence on excitation wavelength. Sensitivity was estimated as a peak-to-peak value from THz electric field transients. LT-GaAs detector sensitivity at 800nm is shown too (filed triangle).

Figure 16 shows the same THz pulse measured with two GaAsBi photoconductive detectors manufactured from different layers and activated with 150 fs duration laser pulses at various wavelengths. It can be seen from that figure that the sensitivity of both GaAsBi detectors is highest when it is illuminated with 1 to 1.2 eV photon energies. The sensitivity of both detectors falls rather abruptly at 1.2 eV. The most pronounced difference of both photosensitivity spectra is evident on their small photon energy side. For detector A, the sensitivity falls to zero at 0.9 eV, whereas for detector B, illuminated 0.8 eV laser pulses, the detected amplitude of THz transient is only by 40% lower than its maximum. THz transients of rather significant amplitude were detected with this device even at 0.6 eV.

It is known that thick layers of GaAsBi are often inhomogeneous and contain different Bi-related defects and clusters with different bismuth contents [41]. Figure 17 presents optical absorption spectra measured on both investigated GaAsBi layers. These spectra contain tails extending up to 0.75 eV for sample A and 0.7 eV (or even smaler) for sample B which are most probably related to the inhomogeneities mentioned above. It can be observed that the absorption coefficient of sample B is larger too, which could explain a higher sensitivity of sample B at long excitation wavelengths. As bismuth incorporated into alloy modifies mainly its valence band characteristics, whereas the conduction band offsets are much smaller, the electron transport properties in GaAsBi will be less affected by these inhomogeneities. Electrons photoexcited with sub-bandgap photons in the regions with a larger Bi content will propagate in the conduction band with a considerable mobility. This effect can explain the unusually large photoconductivity at the wavelengths of the sampling laser optical pulse, much larger than the apparent optical absorption edge.

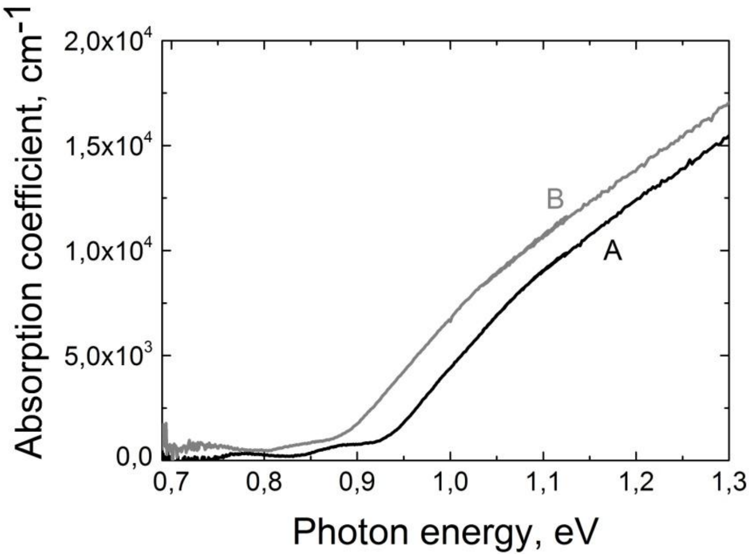

Fig. 17 Optical absorption spectra of A and B GaBiAs layers. Curves at 0.7 eV are noisy due to decreased sensitivity of Ge photo detector at these wavelengths. Reduced absorption coefficient at 0.83 eV (A sample) and 0.8 eV (B sample) are due to Fabry–Perot resonance in these layered structures

The sharp decrease of the THz transient amplitude after the detector excitation with pulses with 1 μm and shorter wavelength is most probably caused by the fact that, nonequilibrium electrons are excited to excess energies higher than the energy position of the subsidiary conduction band L or X valleys with a large electron effective mass, and significantly lower mobility than in the main Γ valley. As the electron energy relaxation time is longer than the duration of the THz pulse, electrons excited with short wavelength photons remain in the low-mobility valleys during the sampling time and the detector sensitivity is low. This experimental observation can be used for the estimation of the energy position of subsidiary conduction band valleys. By taking into account momentum and energy conservation relations, intervalley separation in the conduction band can be obtained. In GaAsBi it was equal to 0.26–0.29 eV.

The THz detector manufactured from layer B was employed in the TDS system based on the femtosecond Er-doped fiber laser (Toptica) with the pulse duration of 80 fs, pulse repetition rate of 80 MHz, and wavelength of 1.55 μm. As in previous experiments, the emitter was a p-type InAs crystal. The average laser beam power used for the emitter excitation was 200 mW. 50 mW of the average fiber laser power was used for the photoexcitation of the THz detector. A THz pulse and its Fourier spectrum are shown in Fig. 18. The spectral width of 2 THz can be seen from that figure even when limited power of an unbiased InAs surface emitter excitation was used. With a more powerful THz emitter, e.g., a photoconductive antenna, and GaAsBi detector, a system with a higher signal-to-noise ratio and a broader THz spectrum could be obtained.

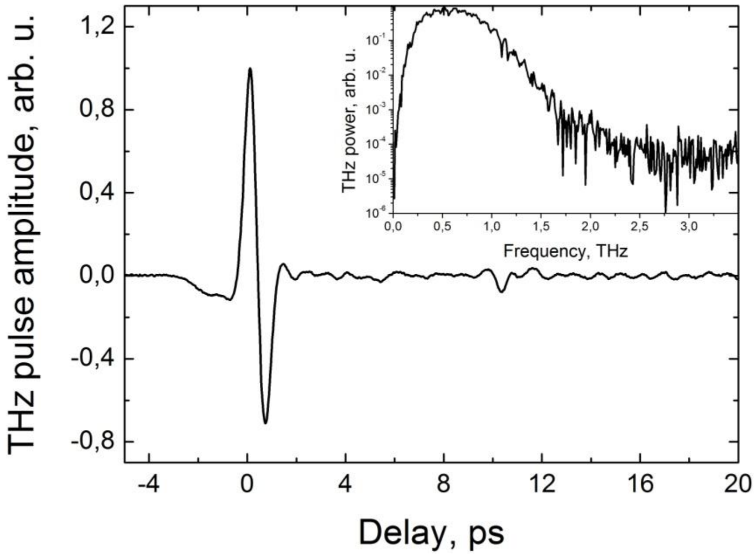

Fig. 18. (a) THz transients and (b) its Fourier spectra of THz-TDS system with GaBiAs detector and p-InAs emitter excited with Er-doped fiber laser emitting at 1.55 μm.

Conclusions

- When the excitation wavelength decreases, amplitude of THz pulses generated at the semiconductor surface grows until reaches the maximum value, which can be used for the determination of subsidiary valley position.
- Subsidiary L valley positions of conduction band were determined from THz excitation spectra of InSb, InAs and GaAs crystals and are equal to 0.55, 1.08, 0.29 eV respectively.
- THz generation efficiency of InAs nanowires depends on their diameter and length and as they increases, it becomes larger.
- In contrast to bulk p-InAs, the main mechanism responsible for THz pulse generation in InAs nanowires is the photo-Dember effect.
- Two different mechanisms are responsible for THz pulse generation from Te surface: photo-Dember effect and anisotropic photoconductivity.
- When Te surface is excited by femtosecond pulses with photon energy lower than 0.9 eV, anisotropic photoconductivity effect dominates. Above 0.9 eV scattering to subsidiary valley of electrons and holes takes place, therefore lateral photo-Dember effect is prevailing THz generation mechanism.
- Picosecond photoconductivity spectra of three low temperature grown semiconductors were measured. Defect band positions of LT-GaAs and LT-$In_{0.3}Ga_{0.7}As$ were determined from these spectra and are 0.77 eV and 0.4 eV respectively. The width of this band is approximately the same in both materials and equal to 68 meV.
- THz-TDS system activated by 1.55 μm femtosecond fiber laser was developed.

References

[1] P. Gu,M. T. S. Kono, and K. Sakai, *J. Appl. Phys.*, **91**, 5533(2002)

[2] H. Dember, Phys. Zeits., **32,** 554 (1931).

[3] X.-C. Zhang, D.H. Auston, *J. Appl. Phys*., **71**, 326 (1992).

[4] V. I. Zemskii, B. P. Zakharchenya, and D. N. Mirlin, *Pis'ma Zh. Eksp. Teor. Fiz*., **24**, 96 (1976) [*JETP Lett.*, **24**, 82 (1976)].

[5] Y. V. Malevich, R. Adomavičius, A. Krotkus, V. L. Malevich, *J. Appl. Phys.*, **115**, 073103 (2014).

[6] G. H. Glover, *J. Appl. Phys.*, **44**, 1295 (1973).

[7] Y. V. Malevich, R. Adomavičius, A. Krotkus and V. L. Malevich, *J. Appl. Phys.*, **115**, 073103 (2014).

[8] R. Adomavičius, G. Molis and A. Krotkus, *Appl. Phys. Lett.*, **87**, 261101 (2005).

[9] A. Bičiūnas, Y. V. Malevich and A. Krotkus *Electron. Lett.*, **47**, 1186 (2011).

[10] R. Ascázubi, I. Wilke, K. Denniston, H. Lu and W. J. Schaff, *Appl. Phys. Lett.*, **84**, 4810 (2004).

[11] Xu G et. Al. *Semicond. Sci. Technol.*, ***25***, 015004 (2010).

[12] P. Carrier and S.-H. Wei, *J. Appl. Phys*., **97**, 033707 (2005)

[13] X.-C. Zhang, D.H. Auston, *J. Appl. Phys*., **71**, 326 (1992).

[14] J. N. Heyman, N. Coates, A. Reinhardt and G. Strasser, *Appl. Phys. Lett.*, **83,** 5476 (2003)

[15] http://www.ioffe.ru/SVA/NSM/Semicond/GaAs/bandstr.html

[16] R. Adomavičius, A. Urbanowicz, G. Molis, A. Krotkus and E. Šatkovskis, *Appl. Phys. Lett.* 85, 2463 (2004)

[17] J. Treu, M. Bormann, H. Schmeiduch, M. Döblinger, M. Morkötter, S. Matich, P. Wiecha, K. Saller, B. Mayer, M. Bichler, M.-C. Amann, J. J. Finley, G. Abstreiter, G. Koblmüller, *Nano Lett.*, **13**, 6070 (2013).

[18] T. Yang, S. Hertenberger, S. Morkötter; G. Abstreiter, G. Koblmüller, *Appl. Phys. Lett.*, **101**, 233102 (2012).

[19] S. A. Dayeh, E. T. Yu, D. Wang, *Small*, **5**, 77 (2009)

[20] A. Lin, J. N. Shapiro, A. C. Scofield, B. L. Liang, D. L. Huffaker, *Appl. Phys. Lett.*, **102**, 053115 (2013).

[21] H. H. Wieder, *Appl. Phys. Lett.*, **25**, 206 (1974).

[22] Y. V. Malevich, R. Adomavičius, A. Krotkus, V. Pačebutas and V. L. Malevich, *JETP Letters*, **101**, 108 (2015).

[23] M. Reid, I. V. Cravetchi, R. Fedosejevs, *Phys. Rev. B*, **72**, 035201 (2005).

[24] T. Dekorsy, H. Auer, H. J. Bakker, H. G. Roskos, and H. Kurz, *Phys.Rev.B*
53, 4005 (1996).

[25] R. Asauskas, V. Balynas, Z. Dobrovolskis, A. Krotkus, and W. Hoerstel, *J. Phys.* **42**, C7-329 (1981).

[26] P. Grosse, *Die Festkoerper Eigenschaften von Tellur*, Springer-Verlag, Berlin (1969).

[27] E. L. Ivchenko and G. E. Pikus, *JETP Lett.* 27, 604 (1976).

[28] I. P. Zhadko, E. I. Rashba, V. A. Romanov, I. M. Stakhira and K. D. Tovstyuk, *Sov. Phys. - Solid State* **7**, 1432 (1965).

[29] V. L. Malevich, P. A. Ziaziulia, R. Adomavicius, A. Krotkus, and Y. V. Malevich, *J. Appl. Phys.* **112**, 073115 (2012).

[30] G. Ribakovs and A. A. Gundjian, *J. Appl. Phys.*, **48**, 4601 (1977).

[31] V. L. Malevich, A. Krotkus, A. Bičiunas, and V. Pačebutas, *J. Appl. Phys.*, **104**, 113117 (2008).

[32] H. Shen, F. C. Rong, R. Lux, J. Pamulapati, M. Taysing-Lara, M. Dutta, E. H. Poindexter, L. Calderon, and Y. Lu, *Appl. Phys. Lett.*, **61**, 1585 (1992).

[33] J. Lagowski, *Appl. Phys. Lett.* **40**, 342 (1982).

[34] W. C. Hurlbut, Y.-S. Lee, K. L. Vodopyanov, P. S. Kuo, and M. M. Fejer, Opt. Lett.32, 668 (2007).

[35] S. U. Dankowski, D. Streb, M. Ruff, P. Kiesel, M. Kneissl, B. Knüpfer, G. H. Döhler, U. D. Keil, C. B. Sorenson, and A. K. Verma, *Appl. Phys. Lett.*, **68**, 37 (1996).

[36] M. C. Nuss, D. H. Auston, and F. Capasso, *Phys. Rev. Lett.*, **58**, 2355 (1987).

[37] H. Němec, A. Pashkin, P. Kužel, M. Khazan, S. Schnull, and I. Wilke, *J. Appl. Phys.* 90, 1303 (2001).

[38] P. A. Rolland, E. Constant, E. Salmer, and R. Fauquem-bergue, *Electron. Lett.*, **15**, 373 (1979).

[39] Sheng. S. Li, *Semiconductor Physical Electronics*, Plenum Press, New York and London, , pp. 191–201 (2006).

[40] V. Pačebutas, A. Bičiūnas, S. Balakauskas, A. Krotkus, G. Andriukaitis, D. Lorenc, A. Pugžlys, and A. Baltuška, *Appl. Phys. Lett.* **97**, 031111 (2010).

[41] S. Imhof, C. Wagner, A. Chernikov, M. Koch, K. Kolata, N. S. Köster, S. Chatterjee, S. W. Koch, X. Lu, S. R. Johnson, D. A. Beaton, T. Tiedje, O. Rubel, and A. Thränhardt, *Phys. Status Solidi B,* **248**, 851 (2011).

List of publications

- Andrius Arlauskas, Arūnas Krotkus, THz excitation spectra of AIIIBV semiconductors, Semicond. Sci. Technol. **27** (2012) 115015.
- Andrius Arlauskas, Polina Svidovsky, Klemensas Bertulis, Ramūnas Adomavičius, Arūnas Krotkus, GaAsBi Photoconductive Terahertz Detector Sensitivity at Long Excitation Wavelengths, Appl. Phys. Express **5** (2012) 022601.
- Andrius Arlauskas, Julian Treu, Kai Saller, Ieva Beleckaitė , Gregor Koblmüller, Arūnas Krotkus, Strong Terahertz Emission and Its Origin from Catalyst-Free InAs Nanowire Arrays, NanoLett. **14** (2014) 1508.
- Bičiūnas, A. Arlauskas, J. Adamonis, P. Cicėnas, Physical mechanisms of terahertz pulse emission from photoexcited surfaces of tellurium crystals, A. Krotkus, J. Appl. Phys. **116** (2014) 093102.
- J. Adamonis, A. Arlauskas, A. Krotkus, Spectral measurements of picosecond photoconductivity in terahertz detectors made from low temperature grown GaAs and GaInAs, Phys. Status Solidi A, 212 (2015) 2080.

Conference presentations

1. A. Arlauskas, R. Adomavičius, J. Adamonis, A. Krotkus, Spectral measurements of the picosecond photoconductivity in semiconductors by THz radiation pulses, 3rd EOS Topical Meeting on Terahertz Science & Technology (2012), Prague.
2. Andrius Arlauskas, Anton Koroliov, Saulius Balakauskas, Martynas Šoliūnas, Rasa Suzanovičienė, Andrius Maneikis, Arūnas Šetkus, Arūnas Krotkus, Vincas Tamošiūnas, Terahercų dažnio spinduliuotės emisijos iš Cu(In,Ga)$(S,Se)_2$ sluoksnių tyrimai, Lietuvos nacionalinė fizikų konferencija 2013, Vilnius.

3. A. Arlauskas, Semiconductors characterization by THz excitation spectroscopy, Jaszowiec 2013 (2013), Poland, Wisla.
4. Andrius Arlauskas, THz emission from InAs nanowire arrays, FTMC mokslinė konferencija (2014), Lietuva, Vilnius.

List of publications not included into doctoral dissertation

1. A. Koroliov, A. Arlauskas, S. Balakauskas, M. Šoliūnas, A. Maneikis, A. Krotkus, A. Šetkus V. Tamošiūnas, Study of Terahertz Emission from Surfaces of Cu(InGa)Se_2 Layers, Acta Phys. Pol. A, **124** (2013), 846
2. Renata Butkutė, Vaidas Pačebutas, Bronislovas Čechavičius, Ramūnas Nedzinskas, Algirdas Selskis, Andrius Arlauskas, Arūnas Krotkus, Photoluminescence at up to 2.4µm wavelengths from GaInAsBi/AlInAs quantum wells, J. Cryst. Growth, **391** (2014) 116.
3. A. Atrashchenko, A. Arlauskas, R. Adomavičius, A. Korotchenkov, V. P. Ulin, P. Belov, A. Krotkus, V. P. Evtikhiev, Giant enhancement of terahertz emission from nanoporous GaP, Appl. Phys. Lett. **105** (2014) 191905

Santrauka

Apšvietus puslaidininkio paviršių femtosekundiniu lazerio impulsu, atspindžio kampu yra sugeneruojamas kelių pikosekundžių trukmės, dažnai vieno periodo elektromagnetinis svyravimas, kurios spektras yra teraherciniame (THz) diapazone. Šios spinduliuotės prigimtis yra susijusi su krūvio judėjimu, kuris vyksta dėl įvairių priežasčių: paviršinis elektrinis laukas, skirtingi krūvininkų difuzijos koeficientai taip pat netiesinai optiniai efektai, fononų svyravimai, optinė krūvininkų orientacija. Natūralu, kad THz impulsas talpina savyje informaciją apie šiuos mechanizmus, o tuo pačiu ir apie krūvininkų dinamiką iškart po sužadinimo. Tad šio darbo tikslas buvo sukurti THz impulsų sužadinimo bei pikosekundinio fotolaidumo spektroskopijos metodikas, kurios leidžia nagrinėti medžiagų juostinę struktūra bei tyrinėti procesus vykstančius iškart po sužadinimo.

Siekiant parodyto THz impulsų sužadinimo spektroskopijos galimybes, šiame darbe buvo išmatuoti 4 medžiagų (InAs, InSb, InN, GaAs) sužadinimo spektrai. Iš jų buvo nustatytos laidumo juostos šoninio slėnio padėtys, kurios gan tiksliai sutapo su literatūroje žinomomis vertėmis.

Šiame darbe pirmą kartą buvo tirta THz impulsų generacija nuo InAs nanovielelių matricos, kurios buvo augintos be katalizatorius. Dėl paviršinių defektų, elektronų judris, kuris tampriai susijęs su THz impulsų generacijos efektyvumu, šiose nanovielėse priklauso nuo jų skersmens. Tuo pačiu dėl gerokai trumpesnės impulso relaksacijos trukmės pakinta ir generacijos mechanizmas. Nustatyta, kad InAs nanovielelėse THz impulsai generuojami dėl foto-Demberio efekto.

Telūras – tai vienas iš nedaugelio puslaidininkių, kurio fononų svyravimų kuriama THz spinduliuotė yra lengvai užregistruojama įprastos TDS sistemos. Šiame darbe buvo ištirti trijų kristalografinių orientacijų Te kristalai. Nustatyta, kad be fononų oscilaicijų egzistuoja dar trys generacijos mechanizmai. Kai puslaidininkis žadinamas mažesnio nei 0,9 eV energijos fotonais, THz generuojami dėl anizotropinio fotolaidumo reiškinio. Kai

fotono energija viršija 0,9 eV, įsijungia dar du: šoninis foto-Demberio efektas, kuris atsiranda dėl elipsoidinio laidumu juostos izoenergetinio paviršiaus, ir įprastas foto-Demberio efektas. Toliau didėjant fotono energijai ima dominuoti pastarieji du.

Paskutinėje šio darbo dalyje buvo pristatyta pikosekudinio fotolaidumo spektroskopijos metodika. Skirtingai nuo įprasto fotolaidumo ši išsiskiria tuo, kad geba nagrinėti nespėjusių termalizuotis elektronų judėjimą bei procesus, kurie vyksta keli šimtai femtosekundžių po sužadinimo. Tuo pačiu ši metodika leidžia įvertinti ir draustinių energijų tarpe esančių lygmenų energijas. Šiame darbe buvo išmatuota trijų medžiagų pikosekundinio fotolaidumo spektrai: žemoje temperatūroje (ŽT) augintas GaAs, ŽT-InGaAs ir GaAsBi. Pirmų dviejų medžiagų draustiniame tarpe yra struktūrinių defektų sąlygota juosta, kurios energetinė padėtis bei plotis buvo įvertintas šia metodika. GaAsBi atveju buvo nustatyta laidumo juostos šoninio slėnio padėtis šioje medžiagoje.

Curriculum Vitae

Name, Surname:	Andrius Arlauskas
Date of birth:	1986 05 08
Place of birth:	Panevėžys, Lietuva
Education:	Date: October 2011 Degree: Master degree in material science Institution: Vilnius University, faculty of physics Date: October 2009 Degree: Bachelor degree Institution: Vilnius University, faculty of physics Date: October 2005 Degree: secondary education Institution: Juozo Balčikonio gymnasium
Scientific experience:	Date: from october 2010 up to now; Position: engineer, young researcher; Institution: Center for Physical Science and Technology ; Date: from september 2012 up to now; Position: Lector; Institution: Vilnius University, faculty of physics; Date: september 2007 – october 2010; Position: engineer; Institution: Institute of Applied Research;
Sumer schools:	42nd International school and conference on the physics and semiconductors, Wisla, Poland June 22nd – 27th 2013
Specialization:	Semiconductor physics, THz science, laser physics, Optoelectronics.